

One-year Observations of Size Distribution Characteristics of Major Aerosol Constituents at a Coastal Receptor Site in Hong Kong: I. Inorganic Ions and Oxalate

Qijing Bian^{1, #}, X. H. Hilda Huang², Jian Zhen Yu^{1,2, *}

¹Department of Chemistry, Hong Kong University of Science & Technology, Clear Water Bay, Kowloon, Hong Kong

²Institute of the Environment, Hong Kong University of Science & Technology, Clear Water Bay, Kowloon, Hong Kong

[#]now at: Department of Atmospheric Science, Colorado State University

Correspondence to: Jian Zhen Yu (jian.yu@ust.hk)
Tel: (852) 2358 7389, Fax: (852) 2358 1594

Abstract

Size distribution data of major aerosol constituents are essential in source apportioning of visibility degradation, testing and verification of air quality models incorporating aerosols. We report here one-year observations of mass size distributions of major inorganic ions (sulfate, nitrate, chloride, ammonium, sodium, potassium, magnesium and calcium) and oxalate at a coastal suburban receptor site in Hong Kong, China. A total of 43 sets of size segregated samples in the size range of 0.056–18 μm were collected from March 2011 to February 2012. The size distributions of sulfate, ammonium, potassium and oxalate were characterized by a dominant droplet mode with a mass mean aerodynamic diameter (MMAD) in the range of ~ 0.7 – $0.9 \mu\text{m}$. Oxalate had a slightly larger MMAD than sulfate on days with temperatures above 22°C as a result of the process of volatilization and repartitioning. Nitrate was mostly dominated by the coarse mode but enhanced presence in fine mode was detected on winter days with lower temperature and lower concentrations of sea salt and soil particles. This data set reveals an inversely proportional relationship between the fraction of nitrate in the fine mode and product of the sum of sodium and calcium in equivalent concentrations and the dissociation constant of ammonium nitrate (i.e., $(1/([\text{Na}^+] + 2[\text{Ca}^{2+}]) \times (1/K_e'))$) when P_{n_fine} is significant ($>10\%$). The seasonal variation observed for sea salt aerosol abundance, with lower values in summer and winter, is possibly linked with the lower marine salinities in these two seasons.

Positive matrix factorization was applied to estimate the relative contributions of local formation and transport to the observed ambient sulfate level through the use of the combined

34 datasets of size-segregated sulfate and select gaseous air pollutants. On average, the
regional/super-regional transport of air pollutants was the dominant source at this receptor
36 site, especially on high sulfate days while local formation processes contributed
approximately 30% of the total sulfate. This work provides field measurement-based
38 evidence for importance of understanding both local photochemistry and regional/super-
regional transport in order to properly simulate sulfate aerosols in air quality models.
40 **Keywords:** secondary inorganic aerosols, Chinese aerosols, regional transport, sea salt
aerosols, coarse aerosol

42 **1. Introduction**

Size distribution of aerosols records information of sources and atmospheric processing of
44 particulates. These characteristics of atmospheric particles directly influence local visibility
and regional radiative forcing. Substantial knowledge has been gained on the size
46 distributions of the major inorganic ions, elemental carbon (EC) and organic carbon (OC) in
the past decade in Hong Kong (HK) and over the adjacent Pearl River Delta (PRD) region in
48 South China (Zhuang et al., 1999a, b; Yao et al., 2003; Huang et al., 2006; Liu et al., 2008;
Yu et al., 2010; Lan et al., 2011). The major species, including sulfate, ammonium, OC and
50 EC, predominantly resided in the droplet mode with mass mean aerodynamic diameter
(MMAD) in the range of 0.56-1.0 μm over this region while nitrate was often observed to
52 have a dominant presence in the coarse mode ($>3.2 \mu\text{m}$) in the coastal areas. In these past
studies, however, there is a lack of concurrent measurements of other data (e.g., gaseous data)
54 (Zhuang et al., 1999b; Huang et al., 2006; Yu et al., 2010; Lan et al., 2011) or only a short
period was covered, e.g., PRIDE-PRD campaign 2004 and 2006 in summer (Liu et al., 2008;
56 Yue et al., 2010). In this work, size-segregated aerosol major constituent data, together with
integrated and comprehensive observations of gaseous and bulk particulate pollutants, were
58 obtained for one-year from March 2011 to February 2012 at the Air Quality Research
Supersite (<http://envr.ust.hk/research/research-facility/background-materials.html>) of the
60 Hong Kong University of Science and Technology (HKUST). The comprehensive dataset
significantly improves the data utility and data interpretation as compared with those in
62 previous size distribution studies. As it will be demonstrated later in this paper, the
measurements of a number of gaseous and particulate matter (PM) pollutants (e.g. CO, SO₂,
64 O₃, PM_{2.5}, etc.) at the same site provide supplementary information for more in-depth
understanding of aerosol sources and processing.
66 Much of this work's focus is on sulfate and nitrate. Sulfate remains a top contributor to

aerosols over the PRD region (He et al., 2011; Huang et al., 2014), although a consensus on
68 SO₂ emission reduction has reached between Hong Kong SAR Government and Guangdong
Provincial Government since 2002
70 ([http://www.epd.gov.hk/epd/english/environmentinhk/air/prob_solutions/strategies_apc.html](http://www.epd.gov.hk/epd/english/environmentinhk/air/prob_solutions/strategies_apc.html#point_1)
[#point_1](#)). This arouses the interest in determining the relative contributions of local
72 formation versus regional/super-regional transport to the observed ambient sulfate loadings.
A number of numerical modeling approaches (e.g. observational based model and source-
74 oriented model) have been applied to identify the source origins of sulfate over this region
(Zhang et al., 2009; Wu, 2013; Xue et al., 2014). The accuracy of the results from these
76 numerical studies heavily relies on whether emission inventory and meteorological dynamics
are properly represented in the models. In this work we attempt to use field measurements of
78 size-segregated chemical composition data and select gaseous pollutants in couple with
receptor modeling to estimate local formation vs. transport contributions.

80 Nitrate is a significant, although less abundant than sulfate, component of PM_{2.5}. It also often
has abundant presence in the coarse particles. A source analysis study by Yuan et al. (2013)
82 using receptor modeling of near 10-year speciated PM₁₀ data found secondary nitrate in PM₁₀
increased by 30% from 1998 to 2007 in HK while a decreasing contribution from vehicle
84 emissions was observed. It is observed that the improvement due to reductions of PM in local
emissions has been offset by an increase in non-local contributions with nitrate being a major
86 species. Yang et al. (2011) reported higher [NO₃⁻]/[SO₄²⁻] ratio in PM_{2.5} in Guangzhou than in
other cities in China and implied that on-road automobiles could be the major contributor.
88 Hence, investigation of the partitioning behaviors of nitrate between coarse and fine modes
through size distribution measurements will help to quantify factors and processes affecting
90 PM_{2.5} nitrate.

The size distribution characterization work reported in this work was conducted at the
92 HKUST supersite. Hong Kong is influenced by contrasting air masses in winter and summer
due to the Asian monsoon system. The HKUST supersite is located upwind of HK on the east
94 coast. During most of time in winter the prevailing wind is from north/northeast. In summer,
the dominant wind affecting the site is mainly from South China Sea with relatively clean air
96 mass. As such, it is an appropriate place to study the influence of air pollution from outside
HK. The primary goal of this work is to understand the sources and processing of major ionic
98 aerosol constituents through analyzing their size distribution measurements for a year at this
coastal receptor site. The size distribution characteristics of major ionic species were
100 discussed in detail in this paper. The year-long data has enabled us to look into the

partitioning behavior of nitrate and the factors affecting its abundance in the fine mode. Attempts were also made to apply Positive Matrix Factorization (PMF) to apportion measured size-segregated sulfate into locally formed and regional sources. EC and OC in these size-segregated samples were also measured. Their size distribution characteristics and the major contributing sources will be reported in a separate paper.

2. Sampling location and chemical analysis

A 10-stage Micro-Orifice Uniform Deposit Impactor (MOUDI, non-rotating version, MSP Corp., Shoreview, MN) aerosol sampler was used to collect size-segregated samples with nominal cut sizes of 18 (inlet), 10.0, 5.6, 3.2, 1.8, 1.00, 0.56, 0.32, 0.18, 0.100, and 0.056 μm . The sampler was located at the HKUST Air Quality Research Supersite (22°20'15.72"N, 114°16'3.23"E, Fig. S1). The inlet was ~2 m above roof (~14 m above sea level) and the sampler was operated at a flow rate of 30 L/min. The flow rate was checked before and after every sampling event. The collection substrates were 47-mm quartz fiber filters, pre-baked at 550 °C overnight before use. Special spacers of 0.05 inch in thickness (MSP Corp., Shoreview, MN) were used between adjacent stages to compensate the shorter jet-to-plate distance due to the thicker quartz filter substrate than aluminum foil, on which characterization of the cut-off size and response factor of each impact stage is based. All the filter samples were stored at -18 °C in a refrigerator before analysis. The sampling was carried out for 24 hours from midnight to midnight next day every 12 days from March 1, 2011 to February 29, 2012. An additional 12 sets of samples were collected on an ad-hoc basis to target high-pollution days, including one set in July, three in August, one in September, three in October, one in November, and three in February, respectively. One field blank sample was taken during each sampling event and analyzed in the laboratory together with the samples. The average gravimetric $\text{PM}_{2.5}$ concentration was $25.9 \pm 17.6 \mu\text{g}/\text{m}^3$ on the sampling days (Huang et al., 2013). Among the 12 ad-hoc samples, one sample was collected on August 4, 2012. On this day, relatively low $\text{PM}_{2.5}$ ($8.8 \mu\text{g}/\text{m}^3$) was recorded, as the predicted influence by the severe typhoon MuiFa did not happen. The $\text{PM}_{2.5}$ concentration for the other 11 ad-hoc samples ranged from 17.6 to $61.8 \mu\text{g}/\text{m}^3$.

The MOUDI samples were analyzed for ionic species. One quarter of each filter substrate was extracted with 3 mL of double de-ionized water in an ultrasonic bath for 30 min and the extract was left at 4 °C in a refrigerator overnight to ensure complete extraction. The extracts were filtered using PTFE syringe filter (0.45 μm , Millipore, Billerica, MA, USA) and then

134 analyzed for ionic species using ion chromatography (IC, Dionex DX-500, Thermo Fisher
Scientific, MA, USA). The anions (i.e., Cl^- , NO_3^- , SO_4^{2-} , $\text{C}_2\text{O}_4^{2-}$) were separated using an AS-
136 11 column and a gradient elution solution of NaOH. The cations (i.e., Na^+ , NH_4^+ , K^+ , Mg^{2+} ,
 Ca^{2+}) were separated using a CS-12A column and methanesulfoinc acid as the elution
138 solution (Yang et al., 2005). Full calibrations were carried out in every batch of the ionic
analysis. The species concentrations were field-blank corrected.

140 Daily $\text{PM}_{2.5}$ sampling was conducted using a mid-volume sampler equipped with 5 sampling
channels (SASS, Met One Instrument, OR, USA) in the same period. The collection
142 substrates installed in the 5 channels include one Teflon filter for gravimetric determination
of $\text{PM}_{2.5}$ mass and element analysis, one nylon filter preceded by a MgO-coated denuder for
144 IC analysis of ionic species, and three pre-baked quartz fibers for EC and OC thermal
analysis. $\text{PM}_{2.5}$ element data (i.e. Silicon) used in this study was obtained from the Teflon
146 filters through analysis using an energy dispersive X-ray fluorescence spectrometer (ED-XRF,
Epsilon 5, PANalytical, the Netherlands). The analytical details of gravimetric measurements,
148 ionic and XRF analysis of the $\text{PM}_{2.5}$ samples were given in the paper by Huang et al. (2014a).
Criteria gaseous pollutants were measured by various gas analyzers including SO_2 (100A,
150 API Inc.), CO (300A, API Inc.) and O_3 (400E, Teledyne Instruments Inc.) from June 2011 to
February 2012. Continuous measurements of inorganic species and their related gas-phase
152 components in the ambient air were provided by a MARGA (Metrohm Applikon, The
Netherlands) (Huang et al., 2014a). Relative humidity (RH), temperature, wind speed and
154 wind direction were recorded by an automatic weather station installed on a 10-meter tower
at the site and are shown in Fig. S2.

156

3. Results and discussion

158 3.1 Comparison between MOUDI and $\text{PM}_{2.5}$ measurement

Ionic species measurements (Cl^- , SO_4^{2-} , NO_3^- , $\text{C}_2\text{O}_4^{2-}$, Na^+ , NH_4^+ , K^+ , Mg^{2+} , and Ca^{2+}) by
160 MOUDI and by the mid-volume $\text{PM}_{2.5}$ sampler were compared in Fig. 1. Concentrations for
the ions in individual size bins up to $3.2\ \mu\text{m}$ were added up and compared with those in $\text{PM}_{2.5}$.
162 Good correlations were found between the two sets of measurements for SO_4^{2-} , Na^+ , and
 NH_4^+ , with $R^2 > 0.90$ and the slopes in the range of 0.9–1.1. Measurement uncertainties aside,
164 additional factors, such as particle bounce, sample handling, and the different size cut points
(i.e., $2.5\ \mu\text{m}$ vs. $3.2\ \mu\text{m}$), could also contribute to deviation from a unity slope (Stein et al.,

166 1994; Howell et al., 1998; Chang et al., 2000; Duan et al., 2005). Na^+ was dominated by the
coarse mode ($> 2.5 \mu\text{m}$) and the amount of Na^+ in the size range of 2.5–3.2 μm could be
168 significant relative to Na^+ in $\text{PM}_{2.5}$. For the less abundant species (i.e. $\text{C}_2\text{O}_4^{2-}$, K^+ , and Cl^-),
the correlation between the MOUDI ($\text{PM}_{3.2}$) and $\text{PM}_{2.5}$ measurements were still reasonably
170 good ($R^2 > 0.6$). R^2 values for Mg^{2+} and Ca^{2+} were 0.48 and 0.36, respectively. The weaker
correlations than those of SO_4^{2-} , Na^+ and NH_4^+ could be explained by the larger measurement
172 uncertainties as a result of their much lower concentration levels.

Comparison of nitrate between MOUDI and $\text{PM}_{2.5}$ measurements indicates under-sampling
174 by MOUDI (Fig. 1), which is an expected result of the semi-volatile nature of nitrate. Volatile
loss of particulate nitrate is anticipated due to the pressure drop in the lower 7–10 stages of
176 the MOUDI sampler while such a loss was avoided in the $\text{PM}_{2.5}$ sampler as the Nylon filter
substrates effectively retain ammonium nitrate. A strong temperature-dependence was also
178 observed in the correlation of nitrate between the two sets of measurements. The correlation
in winter ($R^2 = 0.96$, slope = 1.17) was much better than that in summer ($R^2 = 0.13$, slope = -
180 2.58), reflecting the increased dissociation of ammonium nitrate, thereby more volatile loss of
nitrate at higher ambient temperatures.

182 In summary, the comparisons indicate that the MOUDI measurements for the less volatile
ionic species are reliable while nitrate measurements by MOUDI were subjected to sampling
184 artifacts due to volatile loss. The under-sampling of nitrate was more significant for summer
samples than for the winter samples.

186 **3.2 Size distribution characteristics**

Ambient aerosol size distribution is characterized by multiple modes, i.e. nucleation mode,
188 condensation mode, droplet mode and coarse mode, each of which corresponds to distinct
aerosol sources and formation pathways. For example, particles in the condensation mode are
190 usually relatively fresh aerosols while the droplet mode particles may have gone through in-
cloud processing and are more likely linked to regional/super-regional transport (Meng and
192 Seinfeld, 1994).

The continuous size distributions were inverted from measurements for the limited number of
194 size bins by adapting the Twomey algorithm on the known response function of the cascade
impactor (Twomey, 1975; Winklmayr et al., 1990). Tri-modal log-normal distributions were
196 used to fit the measured data in this work on the assumption that the ambient particle
population is superposition of three log-normal modes (i.e., condensation, droplet, and coarse

198 modes) (Dzubay and Hasan, 1990; Dong et al., 2004). The modal concentrations and
MMADs are listed in Table 1. The fitted size distributions fall into two groups, one group
200 with a dominant condensation mode (Fig. 2a) and the second group with a prominent coarse
mode (Fig. 2b). More details are discussed in the ensuing sections.

202 **3.2.1 Size distributions of NH_4^+ , SO_4^{2-} , $\text{C}_2\text{O}_4^{2-}$ and K^+**

The first group of ionic species, including NH_4^+ , SO_4^{2-} , $\text{C}_2\text{O}_4^{2-}$ and K^+ , share a common
204 characteristic of a dominant droplet mode (Fig. 2a). The size distribution patterns for SO_4^{2-}
and NH_4^+ are very similar, with MMAD of $\sim 0.2 \mu\text{m}$ for the condensation mode, $\sim 0.8 \mu\text{m}$ for
206 the droplet mode, and $4.0\text{--}5.0 \mu\text{m}$ for the coarse mode. The fractions of SO_4^{2-} in these three
modes were 3.0–5.9%, 75–81% and 14–21%, respectively. The percentages of NH_4^+ were
208 3.4–4.7%, 81–89% and 4.2–16%, respectively. The molar ratio of $2\times[\text{SO}_4^{2-}]$ and $[\text{NH}_4^+]$ in
particles of $<3.2 \mu\text{m}$ ($\text{PM}_{3.2}$) was 1.04, indicating that fine sulfate mainly existed in the form
210 of ammonium sulfate.

Air masses influencing HK vary with the shift of synoptic-scale meteorology in PRD from
212 season to season. In this study, the season break-down adopts the definition by Louie et al.
(2005), that is, spring is from March to May, summer is from June to August, fall is from
214 September to November, and winter is from December to February. No significant
seasonality in size distribution pattern was observed for SO_4^{2-} and NH_4^+ . Sulfate and
216 ammonium were most abundant in the spring, mainly due to the increase of mass
concentration in the droplet mode.

218 $\text{C}_2\text{O}_4^{2-}$ shows similar size distribution pattern to that of sulfate. The MMADs of the
condensation, droplet, and coarse modes were $0.1\text{--}0.2$, $0.7\text{--}0.9$ and $4.0\text{--}5.0 \mu\text{m}$, respectively
220 and the mass percentages were 0–8.1%, 73–82% and 18–21%, respectively. Several sources
are known to contribute to the atmospheric presence of oxalate, including secondary
222 formation through the oxidation of oxygenated VOCs (e.g. glyoxal) (e.g, Warneck, 2003;
Carlton et al., 2007); biomass burning (Allen et al., 2004; Kundu et al., 2010), and meat
224 charbroiling (Rogge et al., 1991). Yu et al. (2005) observed good correlations between
ambient oxalate and sulfate measurements across a wide geographical span in East Asia and
226 argued that a common dominant formation pathway, likely in-cloud processing, could explain
the close tracking of the two chemically distinct species. For the samples taken in this work,
228 the correlation between the two species in the $0.56\text{--}1.0 \mu\text{m}$ size bin was good ($R^2=0.69$), in
agreement with the suggestion of the common in-cloud processing formation process.

230 It is noted that the MMAD and standard deviation (σ_g) of the droplet mode oxalate in summer

were noticeably larger than those of sulfate while the MMAD and σ_g values of the two
232 species were similar in the other seasons. This prompted us to examine the mass
concentration ratios of both oxalate and sulfate between the two size bins of 1.0–1.8 μm and
234 0.56–1.0 μm (Fig. 3). It is clear that the SO_4^{2-} ratio between the two size bins was lower than
the $\text{C}_2\text{O}_4^{2-}$ ratio on sampling days with temperature higher than 22°C (mostly in summer)
236 while the ratios for the two species were comparable in the other seasons. Oxalic acid was
reported to partition between gas phase and particles under ambient conditions (Limbeck et
238 al., 2001). The enhanced presence of oxalate in the size range of 1.0–1.8 μm could be
explained by evaporation of oxalic acid from the smaller-size particles followed by
240 condensation onto larger particles due to their higher alkalinity. This evaporation-and-re-
condensation process was proposed by Yao et al. (2002, 2003), Mochida et al. (2003) and
242 Sullivan and Prather (2007). Another possible explanation for the increased supermicron
oxalate is more active photochemical oxidation in the gas phase in summer followed by
244 preferential condensation onto the more alkaline larger particles (Rinaldi et al., 2011; van
Pinxteren et al., 2014).

246 The dominant presence of K^+ in the droplet mode could be explained by that the K^+
containing particles can be easily cloud-activated. The good correlation ($R^2=0.64$) between
248 K^+ and SO_4^{2-} in the size bin of 0.56–1.0 μm supports the suggestion of in-cloud processes.
Condensation mode of K^+ , accounting for a small fraction (1.1–8.6%), may be mostly from
250 fresh biomass burning emissions. K^+ in the coarse mode (20–37%) might originate from sea
salt, soil or the coagulation of small biomass burning particles onto coarse particles.

252 **3.2.2 Size distributions of nitrate, sea salt species, and crustal species**

The second group of ionic species, including NO_3^- , Na^+ , Cl^- , Ca^{2+} , and Mg^{2+} , share a common
254 size distribution characteristic of a prominent coarse mode (Fig. 2b). Both bimodal (one fine
mode and one coarse mode) and tri-modal (i.e., one fine mode and two coarse modes) fitting
256 of the measurement data were carried out. In the case of bimodal lognormal fitting, the
Twomey algorithm would result in skewed log-normal distribution curves (Fig. S3). On the
258 other hand, tri-modal data fitting is able to capture the measured size distributions with three
log-normally distributed particle populations (Fig. 2b). The inverted size distributions for this
260 group of species are therefore represented with one fine and two coarse modes. The
underlying physical basis for the presence of two coarse modes will be discussed in detail in
262 the later section.

The droplet mode MMAD values for all five species ranged from 0.8–1.5 μm . The MMAD of

264 the smaller coarse mode (I) ranged from 3.0–4.2 μm and the larger coarse mode (II) ranged
from 6.8–8.1 μm for sea salt species (Na^+ , Mg^{2+} , and Cl^-). Andreas (1998) summarized that
266 sea spray droplets fall into three types and their respective size ranges are film droplets (0.5–5
 μm), jet droplets (3–50 μm) and spume droplets (>20 μm). Film droplets are ejected due to
268 the rupturing of film-thin top of oceanic bubbles on the surface of sea; jet bubbles are formed
from the bottom of surface bubbles after their burst; and spume droplets are produced when
270 the wind tears sea water right off the wave crests. The two coarse modes retrieved for the sea
salt species likely correspond to film droplets and jet droplets. Sea salt particles of spume
272 droplets are not expected to be captured by MOUDI sampling as this sampler only collects
particles up to 18 μm . And this sea salt particle formation theory also explained the small
274 amount of sea salt in the droplet mode (<2.5 μm).

The mass concentration of sea salt aerosol was averagely lower in the summer and winter
276 than in the spring and fall (Table 1). Wai and Tanner (2004) suggested that sea salt particle
concentration is closely dependent on wind speed and seawater salinity. The wind speed at
278 the site was lower in the summer while the speed in the winter was similar to those in the
spring and fall (Fig. S2). Thus, the wind speed was unlikely a dominant factor affecting the
280 concentration of sea salt aerosols at the sampling site. Thiyagarajan et al. (2002) reported that
salinity in eastern HK was the highest (34‰) in spring, the next highest (32‰) in fall while
282 lower (30‰) in the summer and winter. The lower salinity around HK waters in summer and
winter is due to input of fresh water plumes from the Pearl River and the Yangtze River,
284 respectively (Guan and Fang, 2006; Gan et al., 2009). It is plausible that the higher salinity of
sea water in spring and fall explained the higher abundance of the sea salt ionic species in the
286 atmosphere. Current regional air quality models only consider the influence of wind speed
and RH on the sea salt concentration in the coastal surf zone (Kelly et al., 2010). Our results
288 suggest that the oceanic salinity may need to be considered in the parameterization in sea salt
emissions in air quality models.

290 Soluble Ca^{2+} is the product of soil component (i.e., calcium carbonate) reacting with acidic
gases (e.g., HNO_3) or co-existing acidic aerosol components (e.g., H_2SO_4 , HSO_4^-). The larger
292 coarse mode (MMAD: 7.0–7.7 μm) accounted for a dominant fraction (55–77%), the smaller
coarse mode (MMAD: 3.1–4.0 μm) accounted for 21–37%, and a minor fraction (2–12%)
294 was in the fine mode (Table 1). The smaller coarse mode Ca^{2+} is likely associated with long-
range transported dust particles while the larger coarse mode is mainly associated with
296 locally-produced soil particles. Such a differentiation of two coarse mode dust particles with
respect to different source origins was previously suggested by Husar (2004) and VanCuren

298 et al. (2005). Ca^{2+} in the fine and in the smaller coarse mode was found to correlate strongly
with Si in the collocated $\text{PM}_{2.5}$ samples ($R^2 = 0.54$ and 0.80 , respectively) (Fig. 4) while Ca^{2+}
300 in the large coarse mode had a much weaker correlation with Si in $\text{PM}_{2.5}$ ($R^2 = 0.24$). This
result further supports the hypothesis that the smaller coarse mode Ca^{2+} might be associated
302 with long-range transported dust particles. The mass concentration of Ca^{2+} in spring was
 ~ 1.4 – 2.2 times higher than those in other seasons, indicating the increased influence of dust
304 transported from the North China Plain on HK in this season (Lee et al., 2010).

Nitrate is closely associated with sea salt and dust particles as a result of its formation process
306 through the reactions of acidic HNO_3 gas with alkaline components (e.g., Harrison and Poi,
1983). Fitting the measured nitrate size distributions with three log-normal distributions
308 produces a droplet mode of MMAD in the range of 0.8 – 1.0 μm (2–13%), coarse mode I of
MMAD in the range of 3.0 – 4.2 μm (22–47%), and coarse mode II of MMAD in the range of
310 6.8 – 7.4 μm (41–62%). Unlike other ionic species, the relative abundances of nitrate in
different size modes are highly variable among the seasons. The average percentage of
312 aerosol nitrate in the fine mode (<1.8 μm), denoted as P_{n_fine} thereafter, was significantly
higher in the winter samples (37%) than those in the spring (13%), summer and fall ($\leq 6\%$).

314 3.2.3 Factors affecting fine mode nitrate

Fine mode nitrate is mainly in the form of NH_4NO_3 while the coarse mode nitrate is the
316 product of heterogeneous reaction between gaseous NO_2 or HNO_3 and alkaline species such
as Ca^{2+} and Na^+ (Pakkanen et al., 1996; Yoshizu and Hoshi, 1985). NH_4NO_3 is a thermally
318 unstable species and its abundance in aerosols is governed by the following thermodynamic
equilibrium.

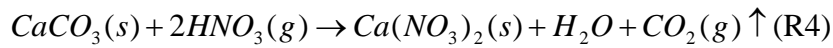
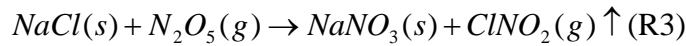


The amount of aerosol NH_4NO_3 is dependent on RH, temperature (T), and concentrations of
322 gas-phase nitric acid and ammonia (Mozurkewich, 1993). Under the RH conditions at the
sampling site (normally larger than 80% during the sampling period) (Fig. S2), calculations
324 using the thermodynamic equilibrium model (i.e. ISORROPIA) show that the nitrate particles
were in the aqueous status.

326 The dissociation constant (K_e) is inherently dependent on RH and T (Mozurkewich, 1993). In
addition, ionic strength of the aerosol aqueous phase also influences the gas-particle
328 partitioning of NH_4NO_3 . For instance, coexistence of SO_4^{2-} in particles reduces K_e in the
 $\text{NH}_4^+/\text{NO}_3^-/\text{SO}_4^{2-}$ system and helps to retain nitrate in the aerosol phase (Stelson and Seinfeld,

1982; Seinfeld and Pandis, 2006). For this reason, a modified dissociation constant K_e' is introduced to take into consideration of the ionic strength effect. K_e' is defined to be the product of K_e and Y , where Y is $[\text{NH}_4\text{NO}_3] / ([\text{NH}_4\text{NO}_3] + 3[(\text{NH}_4)_2\text{SO}_4])$. Our calculations showed that K_e' varied from 0.06 to 5.1 ppb^2 for individual samples and was less than 1.5 ppb^2 for most of the samples collected in spring and winter (Fig. S4). The plot of K_e' vs. P_{n_fine} (Fig. 5a) shows a clear inverse relationship between the two variables, and P_{n_fine} is significant (>10%) only when K_e' falls below 1.0 ppb^2 .

Due to the tendency of gaseous $\text{HNO}_3/\text{N}_2\text{O}_5$ reacting with alkaline sea salt and soil particles (Reactions R2–R4) (Yao and Zhang, 2012), the alkaline species compete for gaseous HNO_3 and thus the abundance of the alkaline species is expected to affect the amount of NH_4NO_3 partitioning onto the fine particles,



The sum of the two major ions (Na^+ and Ca^{2+}) (in equivalent concentrations) is indicative of the abundance of alkaline species on sea salt and soil particles. It is plotted against P_{n_fine} in Fig. 5a and a clear inverse relationship is observed. The coarse mode equivalent concentration of Na^+ and Ca^{2+} was the highest (above 0.2 $\mu\text{eq}/\text{m}^3$) in spring (Fig. S4), which explains the less significant presence of fine mode nitrate in samples collected in spring than those in winter. The following empirical relationship is found between P_{n_fine} and the product of $(1/K_e')$ and $(1 / [\text{Na}^+] + 2[\text{Ca}^{2+}])$ (Fig. 5b):

$$P_{n_fine} = 0.006 \times \left(\frac{1}{K_e'} \right) \times \left(\frac{1}{[\text{Na}^+] + 2[\text{Ca}^{2+}]} \right) + 0.069, R^2 = 0.73$$

Due to the limited sample size and the negative sampling artifact in nitrate by MOUDI, there is a significant degree of scattering in the plot. As shown by Fig. 5b, the fitting equation is largely driven by data points when P_{n_fine} is significant (>10%). As such, whether this equation is applicable to scenarios of small P_{n_fine} can only be evaluated after more and better quality measurements are made in this regime. Nevertheless, this result indicates that in coastal environments, sea salt plays an active role in modulating the amount of nitrate residing in the fine mode particles.

3.2.4 Relationship of coarse mode nitrate formation and chloride depletion

360 Coarse mode nitrate formation and chloride depletion on sea salt particles are closely linked
through reaction R2. The percentages of the chloride depleted ($\text{Cl}^-_{\text{depletion}}\%$) for size bins
362 larger than $3.2\ \mu\text{m}$ were calculated and summarized in Table 2. Generally, the extent of Cl^-
depletion is progressively higher on relatively smaller particles, which is an expected result of
364 more abundant acidic species on the smaller particles. The equivalent ratios of $([\text{Cl}^- + \text{NO}_3^-]) / [\text{Na}^+]$
on coarse particles ranged from 1.20–1.88, which were close to the $[\text{Cl}^-] / [\text{Na}^+]$ ratio
366 in sea water (1.174). It is suggested by Yao and Zhang (2012) that this similarity indicates
that the overall chloride depletion could be largely explained by the coarse mode nitrate
368 formation. MARGA data also showed that the measured HNO_3 (g) and HCl (g) were
moderately correlated in the regime of low $P_{n,\text{fine}}$ (percentage of fine mode nitrate $< 30\%$)
370 (Fig. S5), supporting R2 as a significant pathway for Cl^- depletion.

3.2.5 Comparison of size distributions of secondary ionic species with previous studies

372 Table S1 lists the measurements of MMAD of SO_4^{2-} , NO_3^- , NH_4^+ and $\text{C}_2\text{O}_4^{2-}$ at the HKUST
site in the past decades. MMAD of the condensation mode slightly increased from $\sim 0.2\ \mu\text{m}$ in
374 1996 (Zhuang et al., 1999b) to $\sim 0.3\ \mu\text{m}$ in 2008 (Yu et al., 2010) and in this study. The
MMAD of the droplet mode for sulfate increased from $\sim 0.6\ \mu\text{m}$ in 1996 to $0.8\text{--}0.9\ \mu\text{m}$ in
376 2008 and 2011–2012 (this study). It is difficult to discern whether this observation of shift of
the droplet mode to a large size was incidental (due to the limited measurements and the low
378 temporal resolution in the MOUDI measurements) or reflected increased contributions of
temporal resolution in the MOUDI measurements) or reflected increased contributions of
380 sulfate via regional transport in the recent measurement periods. SO_4^{2-} was neutralized by
gaseous NH_3 in the atmosphere and NH_4^+ thus has the similar variation of size distribution as
382 SO_4^{2-} (Zhuang et al., 1999b; Louie et al., 2005a).

In winter of 1996–1997, coarse-mode nitrate was dominant, with a MMAD of $3.95\ \mu\text{m}$ while
384 in the winter of 2008 and in 2011–2012, nitrate exhibited bimodal distributions. The fine
mode nitrate concentration was 0.58 , 1.01 and $1.43\ \mu\text{g}/\text{m}^3$ in the three periods, respectively.
386 The average concentration of the gaseous precursor (NO_x) was ~ 7.7 ppb in the winter of 1999
and 2000, ~ 13.8 ppb in the winter of 2008 and ~ 10.3 ppb in this study, respectively. The
388 increasing concentration level of NO_x would lead to higher local production of HNO_3 . It is
likely that alkaline species were insufficient to neutralize the increased HNO_3 or NO_3^- and
390 thus a larger proportion of HNO_3 partitions to the fine particles.

No oxalate concentration was reported in the dataset of 1996–1997. MMADs in the
392 condensation mode, droplet mode and coarse mode of this species were comparable in 2008
and 2011-2012.

394 **3.3 PMF analysis of size-segregated sulfate with selected gaseous pollutants**

Multivariate receptor modeling has been widely used to identify underlying emission sources
396 and formation processes and to estimate source contributions to measured ambient particulate
concentration. Several studies have succeeded in applying factor analytic algorithms (Positive
398 Matrix Factorization (PMF) and Multilinear Engine (ME-2)) to size distribution
measurements to retrieve source contribution on the assumption of a unique size distribution
400 for each contributing source and linearity between particle number and mass concentration
over time at a fixed site (Kim et al., 2004; Zhou et al., 2004, 2005). In the following analysis,
402 PMF approach was adopted to estimate the relative contributions of local formation and
regional/superregional transport to the observed ambient sulfate.

404 **3.3.1 PMF analysis of size-segregated sulfate**

The 43 sets of size-segregated sulfate concentrations were combined with the gaseous
406 pollutant measurements (CO, SO₂ and O_x) for PMF analysis using EPA PMF3.0. SO₂ is the
gaseous precursor of particulate sulfate. O_x (the sum of NO₂ and O₃) is usually used to
408 evaluate the oxidation capability of ambient atmosphere. CO is generally considered as an
anthropogenic combustion tracer. Diurnal variation of CO at our measurement site was
410 almost flat and no rush hour peak was observed (Fig. S6). This was clearly different from the
diurnal patterns of elemental carbon and NO_x as observed at a roadside location in Hong
412 Kong showing concentration peaks during local rush hours in the morning and in the early
evening (Huang et al., 2014b). Hence, the diurnal pattern of CO rules out vehicular emissions
414 from nearby roads in the vicinity of a few kilometers as a major contributor to at HKUST.
This is reasonable in view of that the roads near HKUST do not carry heavy traffic as the
416 university is located in a low density residential district in Hong Kong. There are no other
obvious combustion sources near the sampling location to the best of our knowledge. When
418 seasonal variations were examined, CO concentrations were observed to be higher in winter
and lower in summer (Fig. S7), consistent with the seasonal pattern of pollutants transported
420 from outside HK to this site. Therefore, CO is used as a tracer for transported pollutants in
this study.

422 The minimum sample size (N) needed for obtaining statistically reliable results by factor
analysis is $30 + (V + 3) / 2$, where V is the number of input species (Henry et al., 1984). In
424 order to reduce the input variables, data from adjacent size bins were grouped together,
reducing the input size-segregated data to the following five size categories: 1) 0.056–0.32
426 μm ; 2) 0.32–0.56 μm ; 3) 0.56–1.0 μm ; 4) 1.0–3.2 μm ; and 5) $> 3.2 \mu\text{m}$. The dataset of 8
measured variables \times 43 samples was then organized as input matrix for PMF analysis.
428 Uncertainty prepared for PMF analysis was set as the sum of analytical uncertainty and 1/3 of
detection limit for lumped sulfate species (Reff et al., 2007) and 30% of the corresponding
430 concentration for CO, SO₂ and O_x. Three to five factors were tested in PMF analysis and the
three-factor solution was found to best explain the sulfate formation. In the four- and five-
432 factor solutions, sulfate in the size category of 1.0-3.2 μm forms a factor without association
with any gas tracers, leaving this factor unexplained. Five different seed values were tested
434 and similar results were obtained. The seed value was eventually set at 123. Bootstrapping on
the base solution reported stable results, with >85 out of 100 bootstrap factors mapped with
436 those in the based run. Fpeak value from -0.5 to 0.5 was examined. Positive Fpeak values
were applied to sharpen the F matrix and to achieve cleaner source profiles. Q values as a
438 function of Fpeak values are plotted in Fig. S8a. An examination of source profiles shows the
application of Fpeak of 0.1 gives the best result.

440 The first factor consists of all sulfate in the size range of 0.056 to 0.32 μm , 72% of sulfate in
the size bin of 0.32–0.56 μm , 48% of SO₂ and 66% of O_x. Particles in the size bin of 0.056–
442 0.32 μm are associated with the condensation process. The abundant presence of sulfate in
this size bin indicates that this factor is associated with freshly formed aerosols. Reaction of
444 SO₂ with OH radical was the major pathway of sulfate formation in the gas phase while H₂O₂
is the dominant oxidant for SO₂ oxidation in the aqueous phase (Seinfeld and Pandis, 2006;
446 Miyakawa et al., 2007). The ratio ($[\text{SO}_4^{2-}] / ([\text{SO}_2] + [\text{SO}_4^{2-}])$) is calculated to be 0.30, close
to the sulfate conversion extent near power plant sources (Wilson, 1981). This further
448 supports the association of this factor with the freshly formed sulfate particles.

The second factor accounts for more than 60% of sulfate in the size from 0.56 to 3.2 μm and
450 nearly 100% of CO. The conversion factor of SO₂ to sulfate in this factor is 0.97, much larger
than that in the first factor. It is noted that nearly all the sulfate in the size range of 1.0-3.2 μm
452 is associated with this factor. A close examination of the size distribution of sulfate (top row
in Fig. 2a) indicates that the droplet mode of sulfate was broad and dominant, encompassing
454 most of sulfate in the 1.0-3.2 μm range. The abundant presence of the super-micron droplet
mode sulfate particles suggests a major contribution from aged air masses which makes

456 possible significant growth in particle size (Guo et al., 2010). These characteristics indicate that this factor is associated with aged sulfate, i.e., sulfate transported from outside HK.

458 Nearly all of particulate sulfate on particles $>3.2 \mu\text{m}$ appeared in the third factor. This factor is therefore identified as sulfate in the coarse mode and its further apportionment to different sources/formation pathways is discussed in the next section.

460 The sum of apportioned sulfate well explains the ambient sulfate measurements (Fig. 7a).
462 The seasonal average contributions from the three PMF-resolved sources are plotted in Fig. 7b. Locally-formed sulfate ranged from 0.11 to $6.7 \mu\text{g}/\text{m}^3$ in individual samples with the higher values occurring in the spring and fall ($\sim 3.0 \mu\text{g}/\text{m}^3$), consistent with the high oxidant potential (O_x) during these two seasons (Fig. S6). Transported sulfate was in the range of 464 $0.10\text{--}17 \mu\text{g}/\text{m}^3$ in individual samples with the highest seasonal average occurring in spring. Seasonal average sulfate in the coarse mode ranged from $0.3\text{--}1.3 \mu\text{g}/\text{m}^3$ with the highest value 468 in spring. The annual average contribution was estimated to be 30% ($2.5 \mu\text{g}/\text{m}^3$) associated with local oxidation of SO_2 , 59% ($4.9 \mu\text{g}/\text{m}^3$) due to sulfate transported from outside HK, and 470 11% ($0.9 \mu\text{g}/\text{m}^3$) sulfate in the coarse mode. In the high sulfate cases (total $[\text{SO}_4^{2-}] > 14.4 \mu\text{g}/\text{m}^3$, the value corresponding to average + one standard variation of the whole data set), the 472 regional/super-regional pollutant transport played a key role, accounting for an average of 68% of total sulfate and 78% of sulfate in fine mode.

474 3.3.2 PMF analysis of coarse-mode sulfate

To further understand the formation pathway and sources of sulfate in the coarse mode, 476 sulfate and other ionic species (Na^+ , Mg^{2+} , NO_3^- , Ca^{2+} , K^+ and NH_4^+) in the coarse mode were organized as input matrix for PMF analysis. $\text{PM}_{2.5}$ Si as a tracer for bulk soil particles (no 478 coarse Si data available) was also included as input data, as its inclusion significantly improves the agreement of PMF-reconstructed and measured Ca^{2+} data. Uncertainties for 480 these variables were set as the sum of analytical uncertainty and 1/3 of detection limit. F_{peak} value from -0.5 to 0.5 was examined and zero was chosen for final solution (Fig. S8b). Four 482 factors were found to reasonably explain the physical meaning of each source (Fig. 8). The seasonal variations in source contributions are shown in Fig. S9 for individual source factors. 484 Prominent Na^+ , Mg^{2+} , K^+ , Cl^- and $\sim 13\%$ of the coarse-mode sulfate appear in the first factor. Na^+ , Mg^{2+} and some of K^+ on particles larger than $3.2 \mu\text{m}$ are considered to be the tracers for 486 sea salt particles. Major ions in sea water with salinity of 35‰ are Cl^- (55.29% in the mass percentage), Na^+ (30.74%), Mg^{2+} (3.69%), SO_4^{2-} (7.75%), Ca^{2+} (1.18%) and K^+ (1.14%) 488 (Millero and Sohn, 1992). The relative abundance of individual species resolved by PMF in

490 this factor agreed fairly well with that in the sea water except that the PMF-derived SO_4^{2-} was about half of that in the sea water (Fig. S10). This factor therefore was identified as fresh sea salt.

492 The second factor consists of 98% of NH_4^+ , 64% of SO_4^{2-} , 23% of NO_3^- , 13% Na^+ , and 11% of Si. The equivalent ratio of NH_4^+ , SO_4^{2-} , and NO_3^- (1.5:1.0:1.0) in this factor indicates that sulfate mainly exists as NH_4HSO_4 and nitrate as NH_4NO_3 . The alkaline species (i.e. Ca^{2+} , Mg^{2+} , and Na^+) in dust and sea salt make it difficult for ammonia to partition into dust and sea salt particles. Considering the abundant presence of NH_4^+ in this factor, we therefore attribute coarse-mode sulfate apportioned to this factor (termed as $[\text{SO}_4^{2-}]_{\text{C}_F2}$ hereafter) to coagulation of fine NH_4HSO_4 and NH_4NO_3 particles with coarse sea salt/ dust particles or re-suspension of dust particles that contain NH_4HSO_4 and NH_4NO_3 , the presence of which in dust could come from dry or wet deposition of ambient aerosols. As Ca^{2+} in the smaller coarse mode (i.e., $[\text{Ca}^{2+}]_{\text{CMI}}$) represents long-range transported dust particles, an association between $[\text{SO}_4^{2-}]_{\text{C}_F2}$ and $[\text{Ca}^{2+}]_{\text{CMI}}$ is anticipated if coagulation of NH_4HSO_4 fine particles is a significant source for $[\text{SO}_4^{2-}]_{\text{C}_F2}$. On the other hand, an association between $[\text{SO}_4^{2-}]_{\text{C}_F2}$ and Ca^{2+} in coarse mode II (i.e., $[\text{Ca}^{2+}]_{\text{CMI}}$) is expected if re-suspension of dust particles is a significant source for $[\text{SO}_4^{2-}]_{\text{C}_F2}$. We next examine correlations of $[\text{SO}_4^{2-}]_{\text{C}_F2}$ with $[\text{Ca}^{2+}]_{\text{CMI}}$ and $[\text{Ca}^{2+}]_{\text{CMI}}$. It is found that the samples fall into two groups. For samples with lower $[\text{SO}_4^{2-}]_{\text{C}_F2}$ (roughly $<0.4 \mu\text{g}/\text{m}^3$, $n = 28$), $[\text{SO}_4^{2-}]_{\text{C}_F2}$ strongly correlates with $[\text{Ca}^{2+}]_{\text{CMI}}$ ($R^2 = 0.68$) (Fig. 9b) while the correlation with $[\text{Ca}^{2+}]_{\text{CMI}}$ is significantly weaker ($R^2 = 0.49$). For samples with higher $[\text{SO}_4^{2-}]_{\text{C}_F2}$ (roughly $>0.5 \mu\text{g}/\text{m}^3$, $n = 13$), on the other hand, a moderate positive correlation ($R^2 = 0.53$, Fig. 9b) exists between $[\text{SO}_4^{2-}]_{\text{C}_F2}$ and $[\text{Ca}^{2+}]_{\text{CMI}}$ while the correlation with $[\text{Ca}^{2+}]_{\text{CMI}}$ is much weaker ($R^2 = 0.23$). The correlation results indicate that both the coagulation process and re-suspended dust particles could be significant sources for $[\text{SO}_4^{2-}]_{\text{C}_F2}$. That PMF failed to resolve these two sources is most likely due to the limited number of sample size.

The third factor is characterized by the abundant presence of nitrate, Ca^{2+} , Si and chloride-depleted sea salt species (Na^+ , Mg^{2+} , and K^+). Heterogeneous reactions of sulfuric acid and nitric acid on sea salt or dust particles (e.g., reactions R2 and R4) are mainly responsible for this source of coarse-mode sulfate. The co-variation of nitrate and chloride-depleted sea salt species suggested the existence of R2 reaction, i.e., chloride in the sea salt was replaced by nitrate in the polluted atmosphere over certain period. Ca^{2+} and Si are the tracers for dust, which may be amalgamated with local aged sea salt after long range transport. This factor thus was identified as the mixture of aged sea salt and dust particles.

524 The fourth factor is identified as fresh dust particles that have not undergone atmospheric processing (such as acidification), as this factor is characterized with abundant Si and Ca^{2+} but little sulfate and absence of nitrate.

526 The comparisons of PMF-reconstructed and measured coarse mode concentrations show R^2 values of linear regression better than 0.95 for NO_3^- , Cl^- , NH_4^+ , Na^+ , and Mg^{2+} , and 0.83 for 528 Ca^{2+} (Table S2). The agreement for coarse sulfate ($R^2 = 0.79$) is weaker but still reasonable (Fig. 9a). This result indicates that the PMF solution captures most of the variation in the 530 coarse-mode sulfate while it also suggests that likely there are sources or processes not properly represented by the input species. The small sample size and lack of direct coarse 532 dust particle tracer data may be the contributing causes for the limitation in the PMF solution for the coarse sulfate.

534 The PMF results show that on average two-thirds of coarse sulfate is NH_4HSO_4 -containing coarse particles ($\sim 0.5 \mu\text{g}/\text{m}^3$) while the other three sources (i.e., sea salt sulfate, dust sulfate, 536 and aged sea salt/ dust particles) make comparable contributions to the remaining one-third coarse sulfate.

538

4. Summary and implications

540 Size distributions of nine ionic species (SO_4^{2-} , NO_3^- , Cl^- , $\text{C}_2\text{O}_4^{2-}$, Na^+ , NH_4^+ , K^+ , Mg^{2+} , and Ca^{2+}) were determined in a total of 43 sets of samples collected at a suburban receptor 542 location over a year. SO_4^{2-} , NH_4^+ , $\text{C}_2\text{O}_4^{2-}$ and K^+ mainly resided in the droplet mode with MMAD of 0.7–0.9 μm . Minor volatilization and repartition of $\text{C}_2\text{O}_4^{2-}$ led to a larger MMAD 544 and a broader size distribution for the droplet mode under conditions of higher temperatures (i.e. over 22°C). Two coarse modes and one droplet mode were inverted for the species 546 associated with sea salt and dust particles, with MMADs of the two coarse modes as 2–4 μm and 6–8 μm , respectively. The smaller coarse mode for Ca^{2+} was likely associated with long- 548 range transported dust particles while the larger coarse mode is mainly associated with locally-produced soil particles. The seasonal variation of ambient sea salt concentrations 550 could be caused by the seasonal fluctuation in the marine salinity. Modifications of the parameterization in sea salt emission and the oceanic salinity in the air quality models are 552 needed in order to improve the model performance.

As a result of interacting with sea salt and dust particles, NO_3^- was generally dominated by 554 the coarse mode. Enhanced presence of nitrate in fine mode was observed on winter days of lower temperature and on days with lower concentrations of sea salt and soil particles. An

556 inversely proportional relationship was established using the data set between the fraction of
nitrate in the fine mode and $(1/[Na^+] + 2[Ca^{2+}]) \times (1/K_e')$, i.e., product of the sum of alkaline
558 ions in equivalent concentrations (Na^+ and Ca^{2+}) and the modified dissociation constant of
ammonium nitrate. This relationship explains the variable characteristics in nitrate size
560 distribution. Due to limited sample size and sampling artifact of nitrate, more measurement is
needed to further study the relationship.

562 Local formation and transport contribution of sulfate were estimated by applying PMF
analysis on the combined datasets of size-segregated sulfate and select gaseous air pollutants
564 (SO_2 , O_x and CO). The regional/super-regional source dominated the observed sulfate at
HKUST, especially on high sulfate days. On average, the regional source contributed 59%
566 ($4.9 \mu g/m^3$) while the locally-formed sulfate accounted for 30% ($2.5 \mu g/m^3$), and the
remaining sulfate ($0.9 \mu g/m^3$) was on coarse mode particles. Further PMF analysis of the
568 coarse mode chemical composition data suggests that most of the coarse-mode sulfate were
contributed by NH_4HSO_4 -containing coarse particles. This source of coarse sulfate has its
570 origin in fine NH_4HSO_4 particles, which is shifted to the coarse mode through coagulation
and/or deposition followed by re-suspension. Results from this study demonstrate the
572 importance of understanding both local photochemistry and regional/super-regional transport
in order to properly model sulfate aerosols.

574

Acknowledgements

576 This work was supported by the Environmental Conservation Funds (ECF) of Hong Kong
(ECWW09EG04). We thank Hong Kong Environmental Protection Department for making
578 available the MARGA data and Prof. Alexis Lau for the criteria gas monitoring data. Bian Q.
also thanks Dr. Liu Zhiqiang for valuable discussion of possible factors driving atmospheric
580 sea salt particulate variability in Hong Kong.

Supporting Information Available

582 Additional information is shown in two tables and ten figures.

References

Allen, A. G., Cardoso, A. A., and da Rocha, G. O.: Influence of sugar cane burning on

- 586 aerosol soluble ion composition in Southeastern Brazil, *Atmos. Environ.*, 38, 5025–5038,
2004.
- 588 Andreas, E. L.: A new sea spray generation function for wind speeds up to 32 ms^{-1} . *J. Phys.*
Oceanogr., 28, 2175–2184, 1998.
- 590 Carlton, A. G., Turpin, B. J. Turpin, Altieri, K. E., Seitzinger, S., Reff, A., Lim, H.-J., and
592 Ervens, B. : Atmospheric oxalic acid and SOA production from glyoxal: Results of aqueous
photooxidation experiments, *Atmos. Environ.*, 41, 7588–7602, 2007.
- Chang, M.C., Sioutas, C., Kim, S., Gong, H., and Linn, W.S.: Reduction of nitrate losses
594 from filter and impactor samplers by means of concentration enrichment. *Atmos. Environ.*,
34, 85-98, 2000.
- 596 Dong, Y., Hays, M.D, Smith, N. D., and Kinsey, J.S.: Inverting cascade impactor data for
size-resolved characterization of fine particulate source emissions, *J. Aerosol Sci.*, 35, 1497-
598 1512, 2004.
- Duan, J.C., Bi, X.H., Tan, J.H., Sheng, G.Y., and Fu, J.M.: The differences of the size
600 distribution of polycyclic aromatic hydrocarbons (PAHs) between urban and rural sites of
Guangzhou, China. *Atmos. Res.*, 78, 190-203, 2005.
- 602 Dzubay, T.G. and Hasan, H.: Fitting multimodal lognormal size distributions to Cascade
Impactor data. *Aerosol Sci. Technol.*, 13, 144-150, 1990.
- 604 Gan, J.P., Cheung, A., Guo, X.G., and Li, L.: Intensified upwelling over a widened shelf in
the northeastern South China Sea, *J. Geophys. Res.*, 114, C09019,
606 doi:10.1029/2007JC004660, 2009.
- Guan, B.X. and Fang, G.H.: Winter counter-wind currents off the southeastern China coast:
608 A review, *J. Oceanogr.* 62, 1-24, 2006.
- Guo, S., Hu, M., Wang, Z.B., Slanina, J., and Zhao, Y.L.: Size-resolved aerosol water-soluble
610 ionic compositions in the summer of Beijing: implication of regional secondary formation,
Atmos. Chem., Phys., 10, 947-959, 2010
- 612 Harrison, R.M. and Pio, C.A.: Size-differentiated composition of inorganic atmospheric
aerosols of both marine and polluted continental origin, *Atmos. Environ.*, 17, 1733-1738,
614 1983.
- Henry, R.C., Lewis, C.W., and Hopke, P.K., Williamson, H.J.: Review of receptor model
616 fundamentals, *Atmos. Environ.*, 18, 1507-1515, 1984.
- Howell, S., Pszenny, A.A.P., Quinn, P., and Huebert, B.: A field intercomparison of three
618 cascade impactors, *Aerosol Sci. Technol.*, 29, 475-492, 1998.
- He, L.-Y., Huang, X.-F., Xue, L., Hu, M., Lin, Y., Zheng, J., Zhang, R., and Zhang, Y.-H.:
620 Submicron aerosol analysis and organic source apportionment in an urban atmosphere in
Pearl River Delta of China using high-resolution aerosol mass spectrometry, *J. Geophys.*
622 *Res.-Atmos.*, 116, D12304, doi: 10.1029/2010JD014566, 2011
- Huang, X.H.H., Bian, Q., Ng, W. M., Louie, P.K.K., and Yu, J.Z.: Characterization of $\text{PM}_{2.5}$
624 major components and source investigation in suburban Hong Kong: a one year monitoring
study, *Aerosol Air Qual. Res.*, 14, 237-250, 2014a.
- 626 Huang, X.H.H., Bian, Q. J., Louie, P. K. K., and Yu, J. Z.: Contributions of vehicular
carbonaceous aerosols to $\text{PM}_{2.5}$ in a roadside environment in Hong Kong, *Atmos. Chem.*
628 *Phys. Discuss.*, 14, 57-93, 2014b.

630 Huang, X.F., Yu, J.Z., He, L.Y., and Yuan, Z.B.: Water-soluble organic carbon and oxalate in
aerosols at a coastal urban site in China: Size distribution characteristics, sources, and
632 formation mechanisms, *J. Geophys. Res.-Atmos.*, 111, D22212, doi:10.1029/2006JD007408,
2006.

634 Huar, R.B.: Intercontinental transport of dust: historical and recent observational evidence,
Springer Verlag, 2004, chapter 11.

636 Kelly, J.T., Bhave, P.V., Nolte, C.G., Shankar, U., and Foley, K.M.: Simulating emission and
chemical evolution of coarse sea-salt particles in the Community Multiscale Air Quality
(CMAQ) model, *Geosci. Model Dev.*, 3, 257-273, 2010.

638 Kim, E., Hopke, P.K., Larson, T.V., and Covert, D.S.: Analysis of ambient particle size
distributions using unmix and positive matrix factorization, *Environ. Sci. Technol.*, 38, 202-
640 209, 2004.

642 Kundu, S., Kawamura, K., Andreae, T.W., Hoffer, A., and Andreae, M.O.: Molecular
distributions of dicarboxylic acids, ketocarboxylic acids and α -dicarbonyls in biomass
burning aerosols: implications for photochemical production and degradation in smoke layers,
644 *Atmos. Chem. Phys.*, 10, 2209-2225, 2010.

646 Lan, Z.J., Chen, D.L., Li, X., Huang, X.F., He, L.Y., Deng, Y.G., Feng, N., and Hu, M.:
Modal characteristics of carbonaceous aerosol size distribution in an urban atmosphere of
South China. *Atmos. Res.*, 100, 51-60, 2011.

648 Lee, Y.C., Yang, X., and Wenig, M.: Transport of dusts from East Asian and non-East Asian
sources to Hong Kong during dust storm related events 1996-2007, *Atmos. Environ.*, 44,
650 3728-3738, 2010.

652 Limbeck, A., Puxbaum, H., Otter, L., and Scholes, M.C.: Semivolatile behavior of
dicarboxylic acids and other polar organic species at a rural background site (Nylsvley, RSA),
Atmos. Environ., 35, 1853-1862, 2001.

654 Liu, S., Hu, M., Slanina, S., He, L.Y., Niu, Y.W., Bruegemann, E., Gnauk, T., and Herrmann,
H.: Size distribution and source analysis of ionic compositions of aerosols in polluted
656 periods at Xinken in Pearl River Delta (PRD) of China, *Atmos. Environ.*, 42, 6284-6295,
2008.

658 Louie, P.K.K., Wastson, J.G., Chow, J.C., Chen, A., Sin, D.W.M., and Lau, A.K.H.: Seasonal
characteristics and regional transport of PM_{2.5} in Hong Kong, *Atmos. Environ.*, 29, 1695-
660 1710, 2005.

662 Meng, Z.Y. and Seinfeld J.H.: On the source of the submicrometer droplet mode of urban and
regional aerosols., *Aerosol Sci. Technol.*, 20, 253-265, 1994.

664 Millero, F.J. and Sohn, M.J., *Chemistry Oceanography*, CRC Press, Boca Raton, FL, 1992.

Miyakawa, T., Takegawa, N., and Kondo, Y.: Removal of sulfur dioxide and formation of
666 sulfate aerosol in Tokyo. *J. Geophys. Res.-Atmos.*, 112, D13209, doi:10.1029/2006JD007896,
2007.

668 Mochida, M., Umemoto, N., Kawamura, K., Uematsu, M.: Bimodal size distribution of C2-
C4 dicarboxylic acids in the marine aerosols, *Geophys. Res. Lett.*, 30, 1672,
doi:10.1029/2003GL017451, 2003.

670 Mozurkewich, M.: The dissociation-constant of ammonium-nitrate and its dependence on
temperature, relative-humidity and particle-size, *Atmos. Environ.*, 27A, 261-270, 1993.

- 672 Pakkanen, T.A., Kerminen, V.M., Hillamo, R.E., Makinen, M., Makela, T., and Virkkula, A.:
674 Distribution of nitrate over sea-salt and soil derived particles - Implications from a field study,
J. Atmos. Chem., 24, 189-205, 1996.
- 676 Reff, A., Eberly, S.I., and Bhave, P.V.: Receptor modeling of ambient particulate matter data
678 using positive matrix factorization: review of existing methods, J. Air Waste Manage. Assoc.
680 57, 146-154, 2007.
- 678 Rindaldi, M., Decesari, S., Carbone, C., and Tsigaridis, K.: Evidence of a natural marine
680 source of oxalic acid and a possible link to glyoxal, J. Geophys. Res., 116, D16204,
doi:10.1029/2011JD015659, 2011.
- 682 Rogge, W. F., Hildemann, L. M., Mazurek, M. A., Cass, G. R., and Simonelt, B. R. T.:
Sources of fine organic aerosol, 1. Charbroilers and meat cooking operations, Environ. Sci.
Technol., 25, 1112–1125, 1991.
- 684 Seinfeld, J. H., and Pandis, S. N.: Atmospheric Chemistry and Physics—From Air Pollution
686 to Climate Change (2nd Edition), John Wiley & Sons, the United State of America, p.311, p.
477, 2006.
- 688 Stein, S.W., Turpin, B.J., Cai, X.P., Huang, C.P.F., and McMurry, P.H.: Measurements of
relative humidity-dependent bounce and density for atmospheric particles using the DMA-
impactor technique, Atmos. Environ., 28, 1739-1746, 1994.
- 690 Stelson, A.W., and Seinfeld, J.H., Thermodynamic prediction of the water activity, NH_4NO_3
692 dissociation-constant, density and refractive-index for the NH_4NO_3 - $(\text{NH}_4)_2\text{SO}_4$ - H_2O System
at 25 °C, Atmos. Environ., 16, 2507-2514, 1982.
- 694 Sullivan, R.C., and Prather, K. A.: Investigations of the diurnal cycle and mixing state of
oxalic acid in individual particles in Asian Aerosol outflow, Environ. Sci. Technol., 8062-
8069, 2007.
- 696 Thiyagarajan, V., Harder, T., and Qian, P.Y.: Effect of the physiological condition of cyprids
698 and laboratory-mimicked seasonal conditions on the metamorphic successes of *Balanus*
amphitrite Darwin (Cirripedia; Thoracica), J. Exp. Mar. Biol. Ecol., 274, 65-74, 2002.
- 700 Twomey, S.: Comparison of constrained linear inversion and an iterative nonlinear algorithm
applied to indirect estimation of particle-size distributions, J. Comput. Phys., 18, 188-200,
1975.
- 702 VanCuren, R. A., Cliff, S.S., Perry, K.D., and Jimenez-Cruz, M.: Asian continental aerosol
704 persistence above the marine boundary layer over the eastern North Pacific: Continuous aerosol
measurements from Intercontinental Transport and Chemical Transformation 2002 (ITCT
2K2), J. Geophys. Res.-Atmos., 110, D09S90, doi:10.1029/2004JD004973, 2005.
- 706 van Pinxteren, D., Neusüß, C., and Herrmann, H.: On the abundance and source contributions
708 of dicarboxylic acids in size-resolved aerosol particles at continental sites in central Europe,
Atmos. Chem. Phys., 14, 3913-3928, doi:10.5194/acp-14-3913-2014, 2014.
- 710 Wai, K.M., and Tanner, P.A.: Wind-dependent sea salt aerosol in a Western Pacific coastal
area, Atmos. Environ., 38, 1167-1171, 2004.
- 712 Warneck, P.: In-cloud chemistry opens pathway to the formation of oxalic acid in the marine
atmosphere, Atmos. Environ., 37, 2423–2427, 2003. Wilson, W.E.: Sulfate formation in point
source plumes: A review of recent field studies, Atmos. Environ., 15, 2573-2581, 1981.
- 714 Winklmayr, W., Wang, H.C., and John, W.: Adaptation of the twomey algorithm to the
inversion of cascade impactor data, Aerosol Sci. Technol., 13, 322-331, 1990.

716 Wu, D.: Numerical study of atmospheric particulate matters: source apportionment to
characterize 3D transport and transformation of precursors and secondary pollutants, Ph.D.
718 thesis, Hong Kong University of Science & Technology, 2013

Xu, L. and Penner, J. E.: Global simulations of nitrate and ammonium aerosols and their
720 radiative effects, *Atmos. Chem. Phys.*, 12, 9479-9504, doi:10.5194/acp-12-9479-2012, 2012.

Xue, J., Yuan, Z., Yu, J. Z., and Lau, A.K.H. An observation-based model for secondary
722 inorganic aerosols, *Aerosol & Air Quality Res.*, 14, 862-878, 2014.

Yang, H., Yu, J. Z., Ho, S.S.S., Xu, J, Wu, W-S., Wan, C.H., Wang, X., Wang, X., and Wang,
724 L., The chemical composition of inorganic and carbonaceous materials in PM_{2.5} in Nanjing,
China, *Atmos. Environ.*, 39, 3735-2749, 2005.

726 Yang, F., Tan, J., Zhao, Q., Du, Z., He, K., Ma, Y., Duan, F., Chen, G., and Zhao, Q.:
Characteristics of PM_{2.5} speciation in representative megacities and across China, *Atmos.*
728 *Chem. Phys.*, 11, 5207-5219, 2011.

Yao, X. H., Fang, M., and Chan, C. K.: Size distributions and formation of dicarboxylic acids
730 in atmospheric particles, *Atmos. Environ.*, 36, 2099-2107, 2002.

Yao, X.H., Fang, M., and Chan, C.K.: The size dependence of chloride depletion in fine and
732 coarse sea-salt particles, *Atmos. Environ.*, 37, 743-751, 2003.

Yao, X.H. and Zhang, L.M.: Chemical processes in sea-salt chloride depletion observed at a
734 Canadian rural coastal site. *Atmos. Environ.* 46, 189-194, 2012.

Yoshizumi, K. and Hoshi, A.: Size distributions of ammonium-nitrate and sodium-nitrate in
736 atmospheric aerosols, *Environ. Sci. Technol.*, 19, 258-261, 1985.

Yu, H., Wu, C., Wu, D., and Yu, J.Z.: Size distributions of elemental carbon and its
738 contribution to light extinction in urban and rural locations in the Pearl River Delta region,
China, *Atmos. Chem. Phys.*, 10, 5107-5119, 2010.

740 Yu, J.Z., Huang, X.F., Xu, J.H., and Hu, M.: When aerosol sulfate goes up, so does oxalate:
Implication for the formation mechanisms of oxalate, *Environ. Sci. Technol.*, 39, 128-133,
742 2005.

Yuan, Z., Yadav, V., Turner, J. R., Louie, P.K.K., and Lau, A.K.H.: Long-term trends of
744 ambient particulate matter emission source contributions and the accountability of control
strategies in Hong Kong over 1998-2008, *Atmos. Environ.*, 76, 21-31, 2013.

746 Yue, D.L., Hu, M., Wu, Z.J., Guo, S., Wen, M.T., Nowak A., Wehner B., Wiedensohler A.,
Takegawa N., Kondo, Y., Wang, X.S., Li, Y.P., Zeng, L.M., and Zhang, Y.H.: Variation of
748 particle number size distributions and chemical compositions at the urban and downwind
regional sites in the Pearl River Delta during summertime pollution episodes, *Atmos. Chem.*
750 *Phys.*, 10, 9431-9439, 2010.

Zhang, H., Li, J., Ying, Q., Yu, J.Z., Wu, D., Cheng, Y., He, K., Jiang, J.: Source
752 apportionment of PM_{2.5} nitrate and sulfate in China using a source-oriented chemical
transport model, *Atmos. Environ.*, 62, 228-242, 2012.

754 Zhou, L., Kim, E., Hopke, P.K., Stainer, C., and Pandis S.N.: Advanced factor analysis on
Pittsburgh particle size distribution data, *Aerosol Sci. Technol.*, 38, 118-132, 2004.

756 Zhou, L., Hopke, P.K., Stainer C.O., Pandis S.N., Ondov J.M., and Pancras J.P.: Investigation
of the relationship between chemical composition and size distribution of airborne particles
758 by partial least squares and positive matrix factorization, *J. Geophys. Res.-Atmos.*, 110,
D07S18, doi:10.1029/2004JD005050, 2005.

- 760 Zhuang, H., Chan, C.K., Fang, M., and Wexler, A.S.: Formation of nitrate and non-sea-salt sulfate on coarse particles, *Atmos. Environ.*, 33, 4223-4233, 1999a.
- 762 Zhuang, H., Chan, C.K., Fang, M., and Wexler, A.S.: Size distributions of particulate sulfate, nitrate, and ammonium at a coastal site in Hong Kong, *Atmos. Environ.*, 33, 843-853, 1999b.

Table 1. Mass mean aerodynamic diameters (MMAD, μm), standard deviation (σ_g) and modal concentrations of ionic species (C_m , $\mu\text{g}/\text{m}^3$) in spring (N=8, N represent number of samples), summer (N=11), fall (N=13) and winter (N=11).

(a)

	Condensation mode			Droplet mode			Coarse mode		
	C_m ($\mu\text{g}/\text{m}^3$)	MMAD (μm)	σ_g	C_m ($\mu\text{g}/\text{m}^3$)	MMAD (μm)	σ_g	C_m ($\mu\text{g}/\text{m}^3$)	MMAD (μm)	σ_g
SO₄²⁻									
*Spring	0.59	0.24	1.31	9.51	0.84	1.51	2.64	5.07	2.07
Summer	0.32	0.25	1.34	5.30	0.83	1.54	0.91	5.13	2.06
Fall	0.56	0.28	1.30	7.30	0.80	1.38	1.63	4.38	2.31
Winter	0.26	0.26	1.25	6.78	0.84	1.50	1.62	5.03	2.16
NH₄⁺									
Spring	0.26	0.24	1.38	3.79	0.82	1.49	0.63	4.92	2.14
Summer	0.14	0.26	1.35	1.94	0.82	1.53	0.09	5.02	2.35
Fall	0.23	0.30	1.30	2.64	0.78	1.36	0.20	4.25	2.51
Winter	0.12	0.26	1.26	2.86	0.84	1.50	0.56	5.06	2.17
K⁺									
Spring	0.03	0.22	2.18	0.23	0.81	1.49	0.10	5.09	2.05
Summer	0.00	0.16	2.17	0.12	0.78	1.63	0.07	5.73	1.77
Fall	0.01	0.28	1.25	0.22	0.81	1.46	0.08	5.89	1.81
Winter	0.02	0.28	1.27	0.34	0.79	1.49	0.09	4.70	2.16
C₂O₄²⁻									
Spring	0.02	0.22	1.35	0.30	0.80	1.66	0.08	4.58	1.81
Summer	0.00	0.12	1.51	0.18	0.92	2.02	0.04	5.25	1.64
Fall	0.03	0.11	2.59	0.27	0.84	1.66	0.07	4.83	1.81
Winter	0.01	0.29	1.28	0.21	0.77	1.49	0.06	4.58	2.12

(b)

	Droplet mode			Coarse mode I			Coarse mode II		
	C_m ($\mu\text{g}/\text{m}^3$)	MMAD (μm)	σ_g	C_m ($\mu\text{g}/\text{m}^3$)	MMAD (μm)	σ_g	C_m ($\mu\text{g}/\text{m}^3$)	MMAD (μm)	σ_g
NO₃⁻									
Spring	0.74	0.91	1.55	2.28	4.18	1.42	2.50	7.38	1.24
Summer	0.09	0.77	2.18	0.44	3.40	1.49	0.87	7.19	1.42
Fall	0.14	1.03	2.61	1.47	4.03	1.45	1.54	7.33	1.25
Winter	1.43	0.88	1.44	0.84	2.96	1.53	1.56	6.83	1.44
Na⁺									
Spring	0.43	0.90	2.06	1.00	4.07	1.43	1.36	7.49	1.28
Summer	0.14	1.21	1.61	0.66	3.62	1.51	0.95	7.37	1.35
Fall	0.16	1.17	1.61	0.72	3.48	1.51	1.45	7.64	1.32
Winter	0.11	1.10	1.73	0.22	3.40	1.38	0.85	7.67	1.39
Mg²⁺									
Spring	0.01	1.24	1.45	0.11	3.32	1.50	0.22	6.92	1.39
Summer	0.01	1.15	1.54	0.06	3.09	1.51	0.15	7.06	1.47
Fall	0.01	1.28	1.54	0.08	3.25	1.53	0.18	7.62	1.33
Winter	0.01	1.11	1.57	0.03	3.15	1.51	0.11	7.62	1.45
Ca²⁺									
Spring	0.11	1.04	2.12	0.27	3.44	1.45	0.50	6.99	1.40
Summer	0.01	1.14	1.50	0.09	3.11	1.45	0.33	7.68	1.47
Fall	0.04	0.85	1.35	0.16	3.96	1.51	0.24	7.59	1.28
Winter	0.02	1.16	1.81	0.10	3.34	1.43	0.33	7.53	1.44
Cl⁻									
Spring	0.09	1.35	1.87	0.26	3.84	1.26	1.67	7.76	1.28
Summer	0.04	1.48	1.76	0.81	3.89	1.46	1.34	7.49	1.32
Fall	0.04	1.59	1.52	0.24	3.56	1.25	1.96	7.89	1.33
Winter	0.05	1.27	1.79	0.10	3.37	1.25	1.01	8.09	1.39

*Spring is defined as the period from March to May, summer is from June to August, fall is from September to November, and winter is from December to February

Table 2. The percentage of Cl depleted in aged sea-salt aerosols ($\text{Cl}_{\text{depletion}}^{\%}$), relative acidity, and ionic ratios in each season

	3.2- 5.6 μm	5.6-10 μm	10-18 μm	>18 μm
Spring				
¹ $\text{Cl}_{\text{depletion}}^{\%}$	68.73	42.82	34.58	39.34
² Relative acidity	1.42	1.26	1.28	1.30
$([\text{Cl}^-]+[\text{NO}_3^-])/[\text{Na}^+]$	1.26	1.38	1.35	1.21
Summer				
$\text{Cl}_{\text{depletion}}^{\%}$	53.76	34.57	28.28	30.81
Relative acidity	1.22	1.21	1.33	1.41
$([\text{Cl}^-]+[\text{NO}_3^-])/[\text{Na}^+]$	1.20	1.36	1.39	1.34
Fall				
$\text{Cl}_{\text{depletion}}^{\%}$	51.04	28.49	18.50	6.27
Relative acidity	1.05	1.07	1.00	1.06
$([\text{Cl}^-]+[\text{NO}_3^-])/[\text{Na}^+]$	1.20	1.29	1.34	1.42
Winter				
$\text{Cl}_{\text{depletion}}^{\%}$	47.24	29.06	18.81	29.67
Relative acidity	1.16	1.15	1.16	1.17
$([\text{Cl}^-]+[\text{NO}_3^-])/[\text{Na}^+]$	1.88	1.53	1.55	1.41

¹ $\text{Cl}_{\text{depletion}}^{\%} = (1.174 [\text{Na}^+] - [\text{Cl}^-]) / 1.174 [\text{Na}^+] \times 100\%$

² Relative acidity = $([\text{NH}_4^+] + [\text{Na}^+] + [\text{Ca}^{2+}] + [\text{Mg}^{2+}] + [\text{K}^+] / ([\text{SO}_4^{2-}] + [\text{NO}_3^-] + [\text{Cl}^-])$

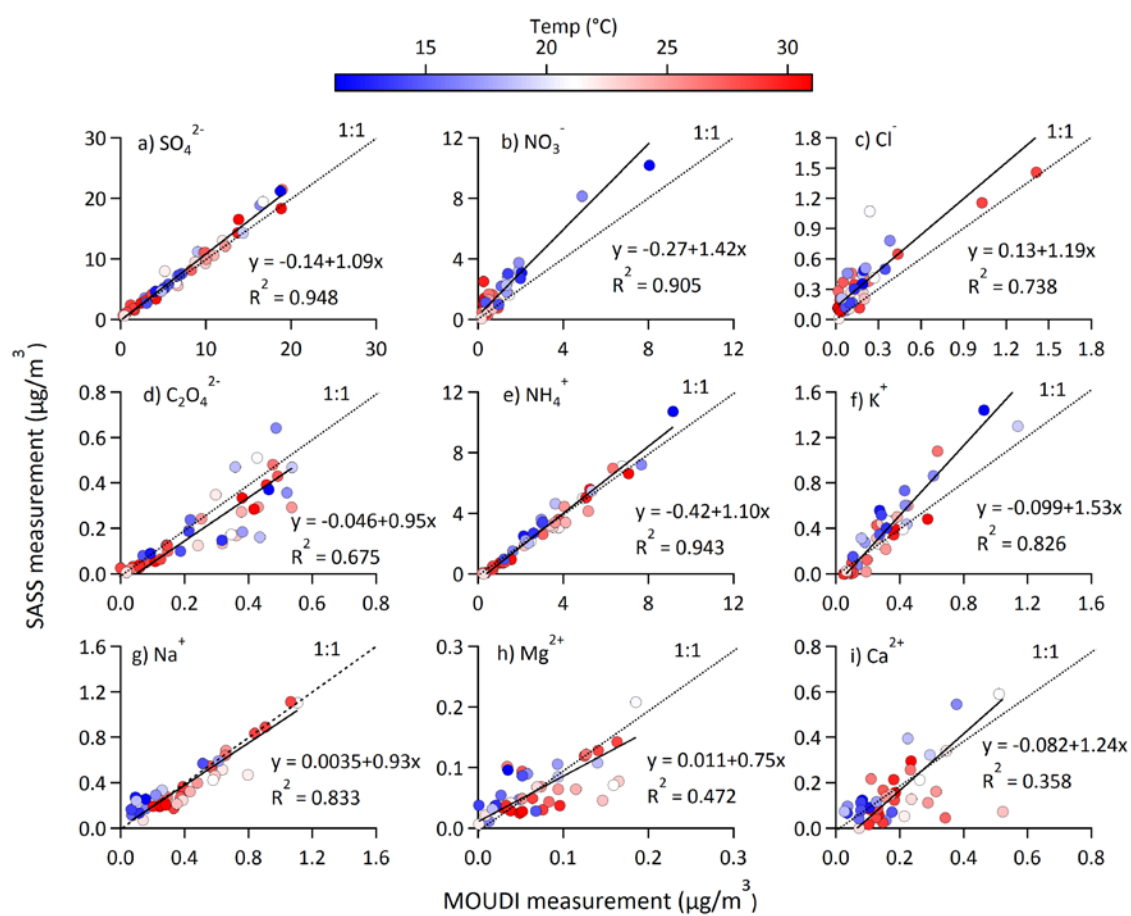
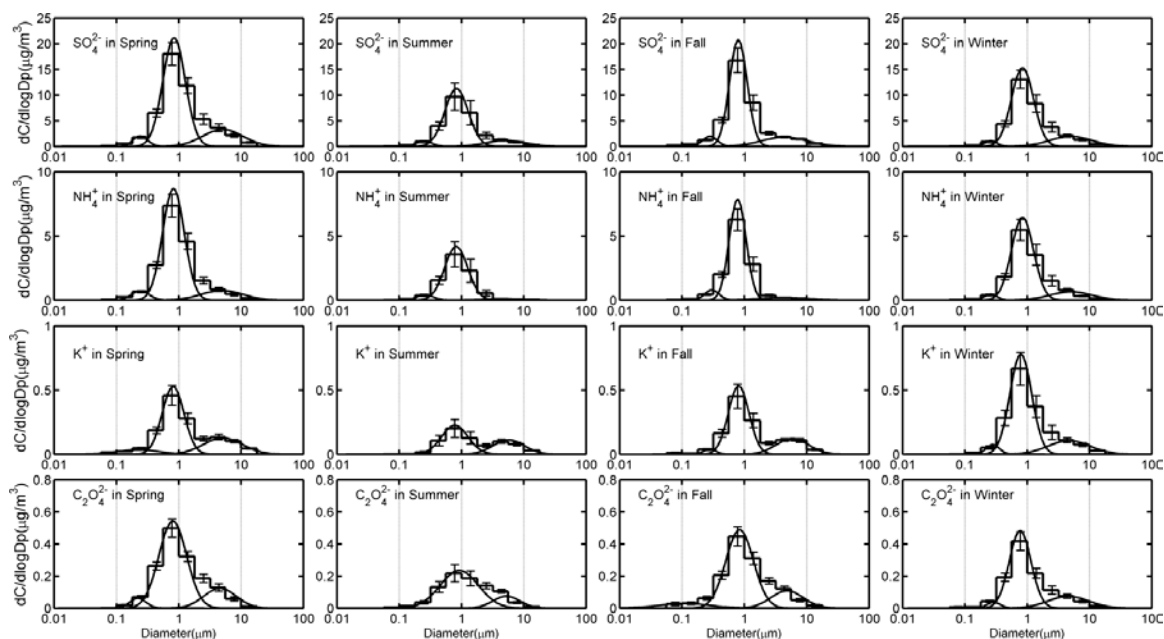
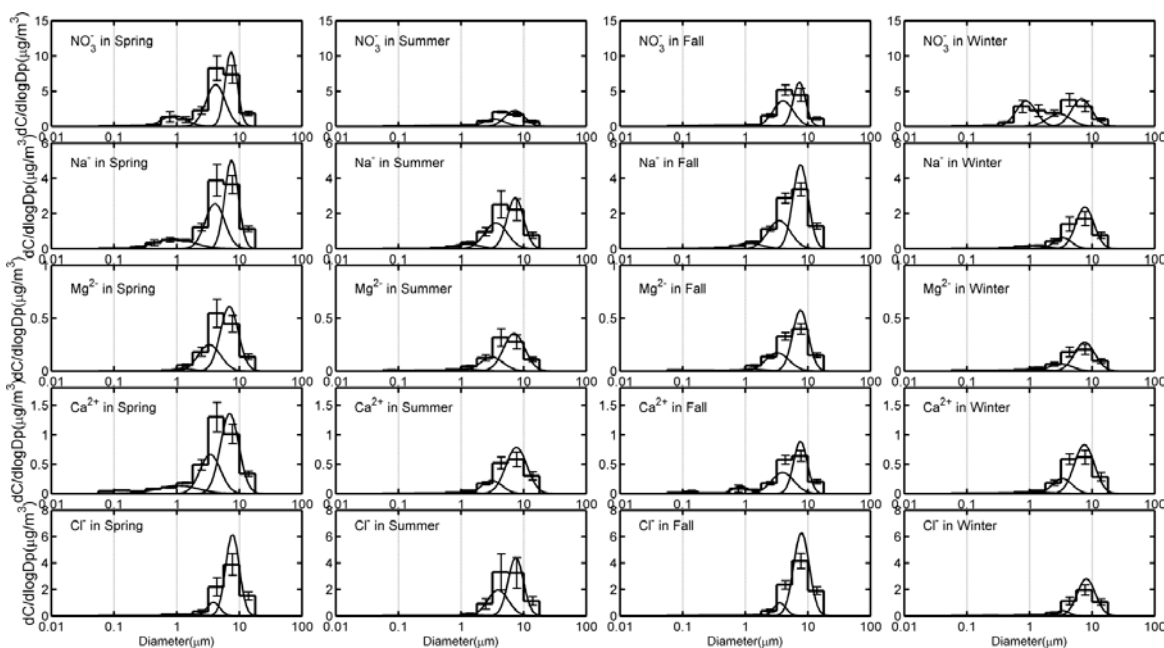


Figure 1. Comparison between MOUDI measurements ($<3.2 \mu\text{m}$) and $\text{PM}_{2.5}$ measurements by SASS sampler. Orthogonal distance regression is applied to examine the comparison. Data points are color-coded by ambient temperatures on the individual sampling days. A segregation of data points by temperature was observed for nitrate, see text for details.



(a)



(b)

Figure 2. Continuous log-normal size distributions of (a) species associated with in-cloud processing (SO_4^{2-} , NH_4^+ , K^+ , $\text{C}_2\text{O}_4^{2-}$) and (b) species associated with crustal and sea salt particles (NO_3^- , Na^+ , Mg^{2+} , Ca^{2+} , Cl^-) in the four seasons. The size distributions are inverted from measured MOUDI data, which are shown in histograms.

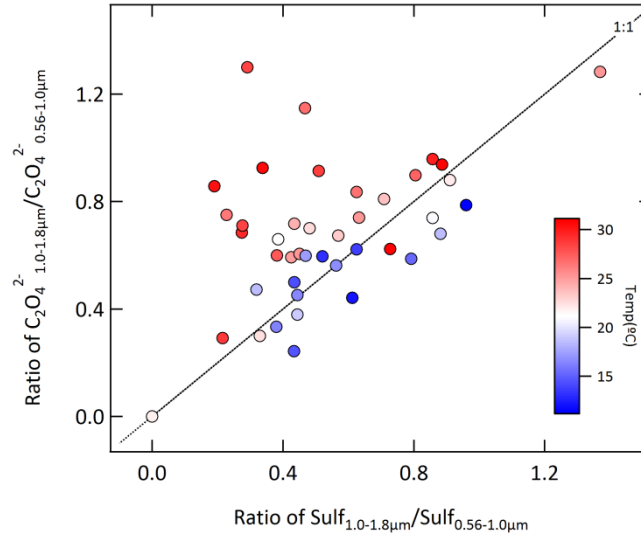


Figure 3. Comparison of mass concentration ratios of oxalate and sulfate between the two size bins 1.0–1.8 μm and 0.56–1.0 μm. The data points are color-coded according to ambient temperature during their collection.

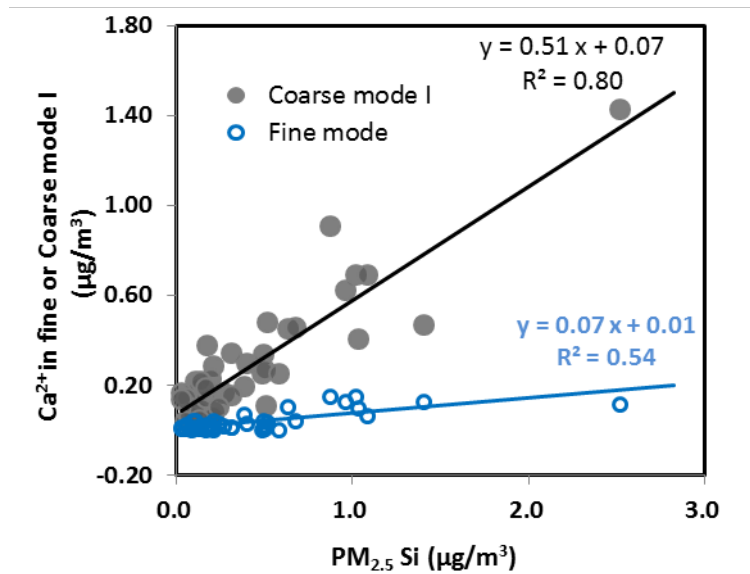


Figure 4. Correlations of Ca²⁺ in fine mode and coarse mode I with Si in collocated PM_{2.5} samples.

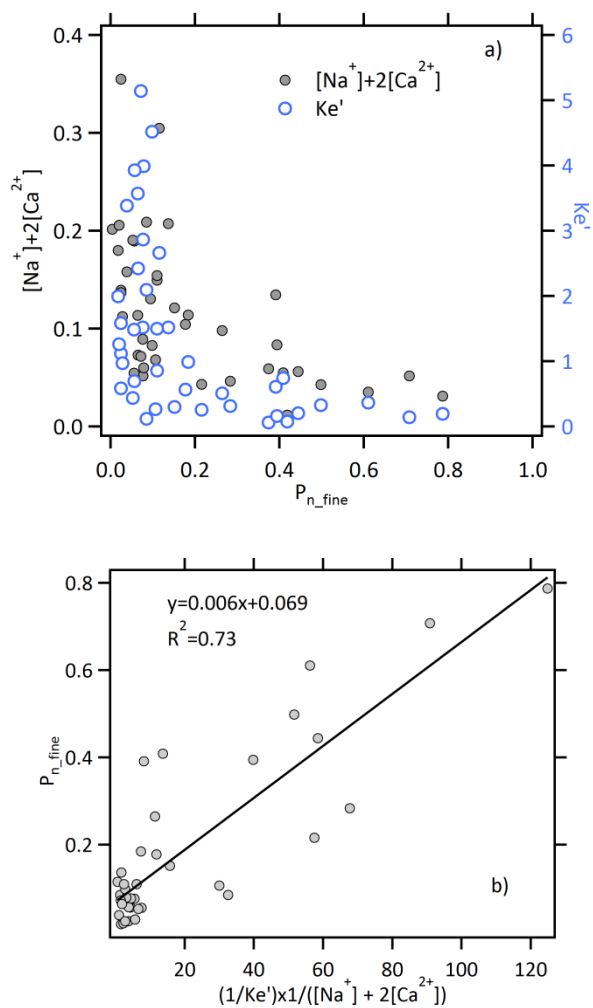


Figure 5. (a) Relationships of aerosol nitrate fraction in the fine mode (P_{n_fine}) ($<1.8 \mu m$) with modified NH_4NO_3 dissociation equilibrium constant (Ke') and equivalent amounts of $[Na^+] + 2[Ca^{2+}]$ in the size range of $>3.2 \mu m$; (b) Empirical relationship between P_{n_fine} and $(1/Ke') \times 1/([Na^+] + 2[Ca^{2+}])$

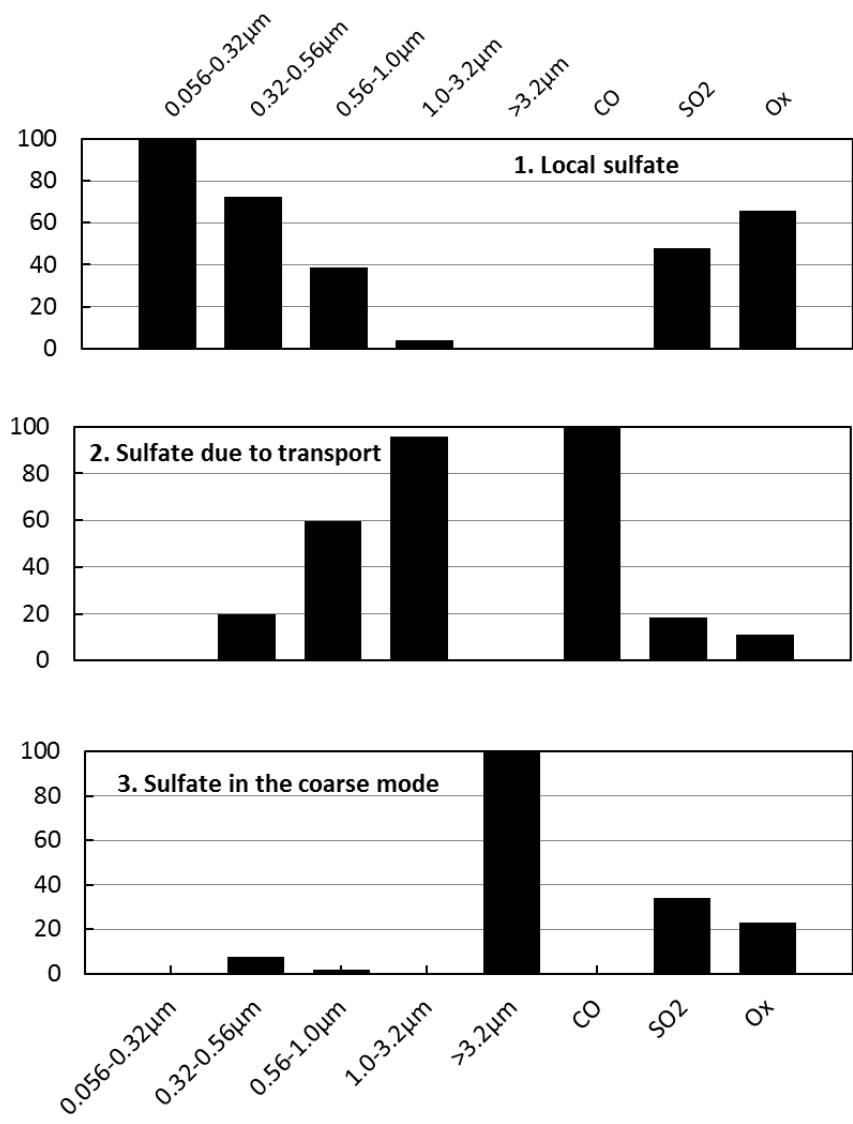


Figure 6. PMF-resolved source profiles (% of total species) for size-segregated SO_4^{2-}

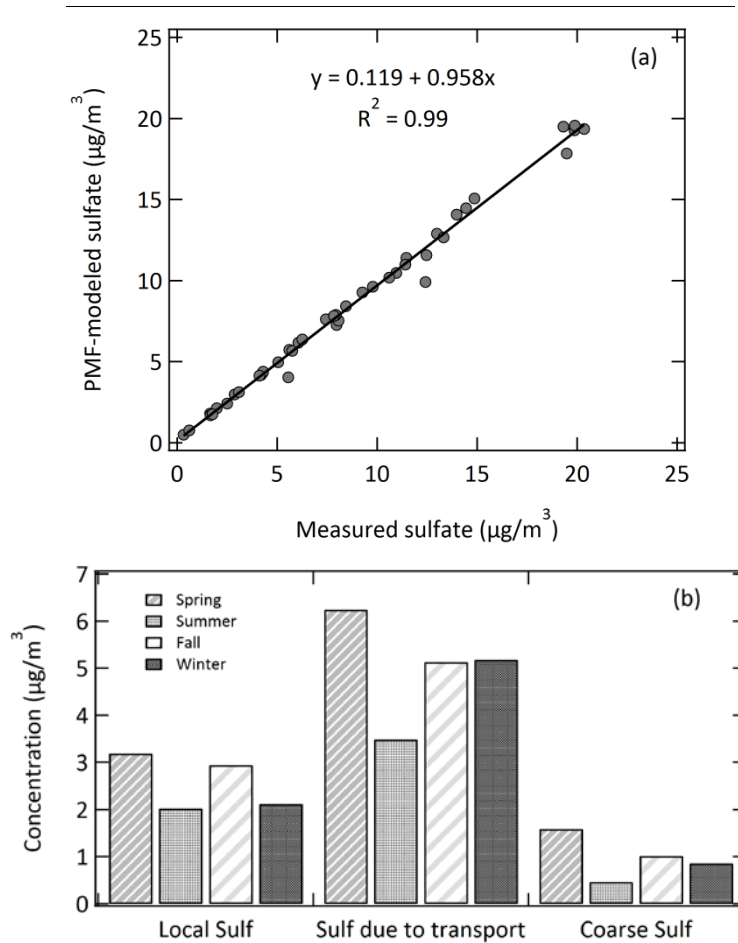


Figure 7. (a) Comparison of PMF-modeled sulfate with the measured sulfate; (b) Seasonal variation in contributions of the three sources to sulfate

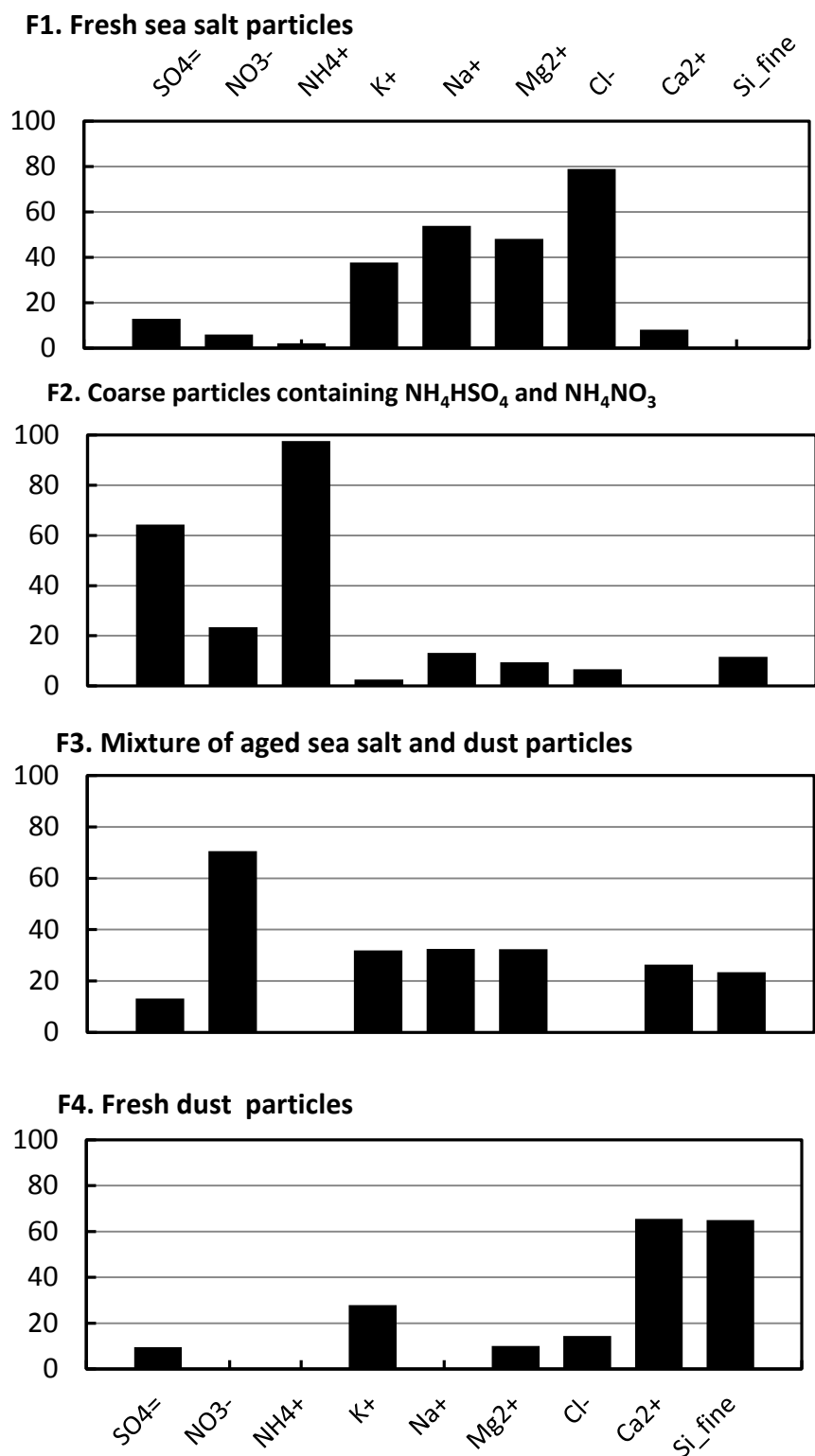


Figure 8. PMF-resolved source profiles (% of total species) for coarse-mode data. PM_{2.5} Si as a surrogate for bulk dust particles is also included as input data.

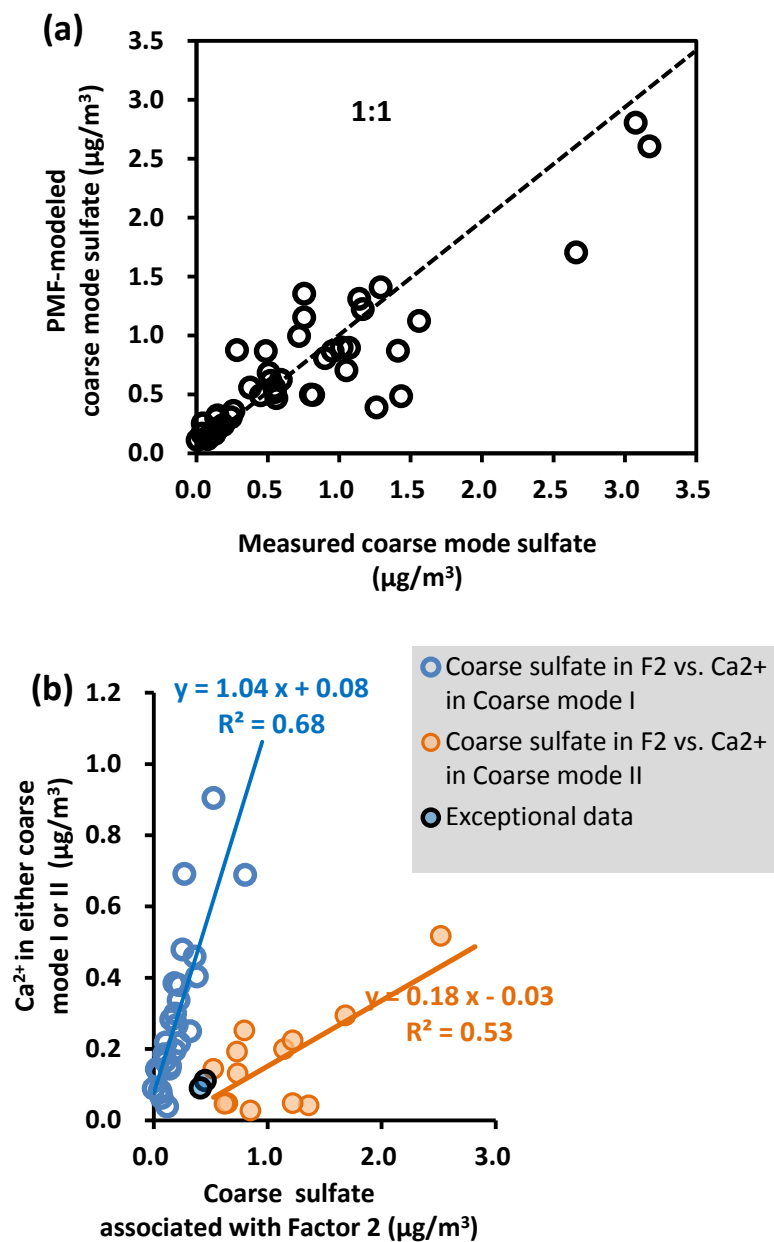


Figure 9. (a) Total sulfate in the coarse mode versus PMF-model estimated sulfate. (b) Relationship of coarse-mode sulfate apportioned to the NH_4HSO_4 -containing coarse particles (i.e., Factor 2) with Ca^{2+} concentration in either Coarse-mode I (blue open circles) or Coarse mode II (yellow filled circles). There are two exceptional data (filled circles with blank outline) that do not fit in either of the two groups.